

Robust Counterfactual Explanations on Graph Neural Networks

Mohit Bajaj^{1*} Lingyang Chu^{2*} Zi Yu Xue^{1,3} Jian Pei⁴
 Lanjun Wang¹ Peter Cho-Ho Lam¹ Yong Zhang¹

¹Huawei Technologies Canada Co., Ltd. ²McMaster University
³The University of British Columbia ⁴Simon Fraser University
 {mohit.bajaj1, zi.yu.xue, lanjun.wang, cho.ho.lam, yong.zhang3}@huawei.com
 chul9@mcmaster.ca, jpei@cs.sfu.ca

Abstract

Massive deployment of Graph Neural Networks (GNNs) in high-stake applications generates a strong demand for explanations that are robust to noise and align well with human intuition. Most existing methods generate explanations by identifying a subgraph of an input graph that has a strong correlation with the prediction. These explanations are not robust to noise because independently optimizing the correlation for a single input can easily overfit noise. Moreover, they are not counterfactual because removing an identified subgraph from an input graph does not necessarily change the prediction result. In this paper, we propose a novel method to generate robust counterfactual explanations on GNNs by explicitly modelling the common decision logic of GNNs on similar input graphs. Our explanations are naturally robust to noise because they are produced from the common decision boundaries of a GNN that govern the predictions of many similar input graphs. The explanations are also counterfactual because removing the set of edges identified by an explanation from the input graph changes the prediction significantly. Exhaustive experiments on many public datasets demonstrate the superior performance of our method.

1 Introduction

Graph Neural Networks (GNNs) [22, 37, 50] have achieved great practical successes in many real-world applications, such as chemistry [31], molecular biology [17], social networks [3] and epidemic modelling [34]. For most of these applications, explaining predictions made by a GNN model is crucial for establishing trust with end-users, identifying the cause of a prediction, and even discovering potential deficiencies of a GNN model before massive deployment. Ideally, an explanation should be able to answer questions like “*Would the prediction of the GNN model change if a certain part of an input molecule is removed?*” in the context of predicting whether an artificial molecule is active for a certain type of proteins [19, 41], “*Would an item recommended still be recommended if a customer had not purchased some other items in the past?*” for a GNN built for recommendation systems [9, 44].

Counterfactual explanations [28] in the form of “*If X had not occurred, Y would not have occurred*” [26] are the principled way to answer such questions and thus are highly desirable for GNNs. In the context of GNNs, a counterfactual explanation identifies a small subset of edges of the input graph instance such that removing those edges significantly changes the prediction made by the GNN. Counterfactual explanations are usually concise and easy to understand [28, 36] because they align well with the human intuition to describe a causal situation [26]. To make explanations more trustworthy, the counterfactual explanation should be robust to noise, that is, some slight changes on

*Equal contribution.

an input graph do not change the explanation significantly. This idea aligns well with the notion of robustness discussed for DNN explanations in computer vision domain [11]. According to Ghorbani et al. [11] many interpretations on neural networks are fragile as it is easier to generate adversarial perturbations that produce perceptively indistinguishable inputs that are assigned the same predicted label, yet have very different interpretations. Here, the concepts of “fragile” “robustness” describe the same concept from opposite perspectives. An interpretation is said to be fragile if systematic perturbations can lead to dramatically different interpretations without changing the label. Otherwise, the interpretation is said to be robust.

How to produce robust counterfactual explanations on predictions made by general graph neural networks is a novel problem that has not been systematically studied before. As to be discussed in Section 2, most GNN explanation methods [45, 25, 46, 37, 32] are neither counterfactual nor robust. These methods mostly focus on identifying a subgraph of an input graph that achieves a high correlation with the prediction result. Such explanations are usually not counterfactual because, due to the high non-convexity of GNNs, removing a subgraph that achieves a high correlation does not necessarily change the prediction result. Moreover, many existing methods [45, 25, 37, 32] are not robust to noise and may change significantly upon slight modifications on input graphs, because the explanation of every single input graph prediction is independently optimized to maximize the correlation with the prediction, thus an explanation can easily overfit the noise in the data.

In this paper², we develop RCExplainer, a novel method to produce robust counterfactual explanations on GNNs. The key idea is to first model the common decision logic of a GNN by set of decision regions where each decision region governs the predictions on a large number of graphs, and then extract robust counterfactual explanations by a deep neural network that explores the decision logic carried by the linear decision boundaries of the decision regions. We make the following contributions.

First, we model the decision logic of a GNN by a set of decision regions, where each decision region is induced by a set of linear decision boundaries of the GNN. We propose an unsupervised method to find decision regions for each class such that each decision region governs the prediction of multiple graph samples predicted to be the same class. The linear decision boundaries of the decision region capture the common decision logic on all the graph instances inside the decision region, thus do not easily overfit the noise of an individual graph instance. By exploring the common decision logic encoded in the linear boundaries, we are able to produce counterfactual explanations that are inherently robust to noise.

Second, based on the linear boundaries of the decision region, we propose a novel loss function to train a neural network that produces a robust counterfactual explanation as a small subset of edges of an input graph. The loss function is designed to directly optimize the explainability and counterfactual property of the subset of edges, such that: 1) the subgraph induced by the edges lies within the decision region, thus has a prediction consistent with the input graph; and 2) deleting the subset of edges from the input graph produces a remainder subgraph that lies outside the decision region, thus the prediction on the remainder subgraph changes significantly.

Last, we conduct comprehensive experimental study to compare our method with the state-of-the-art methods on fidelity, robustness, accuracy and efficiency. All the results solidly demonstrate the superior performance of our approach.

2 Related work

The existing GNN explanation methods [46, 37, 45, 32, 25] generally fall into two categories: model level explanation [46] and instance level explanation [37, 45, 32, 25].

A model level explanation method [46] produces a high-level explanation about the general behaviors of a GNN independent from input examples. This may be achieved by synthesizing a set of artificial graph instances such that each artificial graph instance maximizes the prediction score on a certain class. The weakness of model level explanation methods is that an input graph instance may not contain an artificial graph instance, and removing an artificial graph from an input graph does not necessarily change the prediction. As a result, model level explanations are substantially different from counterfactual explanations, because the synthesized artificial graphs do not provide insights into how the GNN makes its prediction on a specific input graph instance.

The instance level explanation methods [37, 45, 32, 25] explain the prediction(s) made by a GNN on a specific input graph instance or multiple instances by identifying a subgraph of an input graph

²Other versions of the paper are available at <https://arxiv.org/abs/2107.04086>

instance that achieves a high correlation with the prediction on the input graph. GNNExplainer [45] removes redundant edges from an input graph instance to produce an explanation that maximizes the mutual information between the distribution of subgraphs of the input graph and the GNN’s prediction. Following the same idea by Ying et al. [45], PGExplainer [25] parameterizes the generation process of explanations by a deep neural network, and trains it to maximize a similar mutual information based loss used by GNNExplainer [45]. The trained deep neural network is then applied to generate explanations for a single input graph instance or a group of input graphs. MEG [30] incorporates strong domain knowledge in chemistry with a reinforcement learning framework to produce counterfactual explanations on GNNs specifically built for compound prediction, but the heavy reliance on domain knowledge largely limits its applicability on general GNNs. The recently proposed CF-GNNExplainer [24] independently optimizes the counterfactual property for each explanation but ignores the correlation between the prediction and the explanation.

Some studies [32, 37] also adapt the existing explanation methods of image-oriented deep neural networks to produce instance level explanations for GNNs. Pope et al. [32] extend several gradient based methods [33, 35, 49] to explain predictions made by GNNs. The explanations are prone to gradient saturation [12] and may also be misleading [1] due to the heavy reliance on noisy gradients. Velickovic et al. [37] extend the attention mechanism [7, 8] to identify the nodes in an input graph that contribute the most to the prediction. This method has to retrain the GNN with the altered architecture and the inserted attention layers. Thus, the explanations may not be faithful to the original GNN.

Instance level explanations from most of the methods are usually not counterfactual because, due to the non-convexity of GNNs, removing an explanation subgraph from the input graph does not necessarily change the prediction result. Moreover, those methods [45, 25, 37, 32, 24] are usually not robust to noise because the explanation of every single input graph prediction is independently optimized. Thus, an explanation can easily overfit the noise inside input graphs and may change significantly upon slight modifications on input graphs.

To tackle the weaknesses in the existing methods, in this paper, we directly optimize the counterfactual property of an explanation along with the correlation between the explanation and the prediction. Our explanations are also much more robust to modifications on input graphs, because they are produced from the common decision logic on a large group of similar input graphs, which do not easily overfit the noise of an individual graph sample.

Please note that our study is substantially different from adversarial attacks on GNNs. The adversarial attacking methods [51, 53, 42, 43, 20] use adversarial examples to change the predictions of GNNs but ignore the explainability of the generated adversarial examples [10]. Thus, the adversarial examples generated by adversarial attacks may not explain the original prediction.

Our method is substantially different from the above works because we focus on explaining the prediction by directly optimizing the counterfactual property of an explanation along with correlation of the explanation with the prediction. We also require that the explanation is generally valid for a large set of similar graph instances by extracting it from the common linear decision boundaries of a large decision region.

3 Problem Formulation

Denote by $G = \{V, E\}$ a graph where $V = \{v_1, v_2, \dots, v_n\}$ is the set of n nodes and $E \subseteq V \times V$ is the set of edges. The edge structure of a graph G is described by an adjacency matrix $\mathbf{A} \in \{0, 1\}^{n \times n}$, where $\mathbf{A}_{ij} = 1$ if there is an edge between node v_i and v_j ; and $\mathbf{A}_{ij} = 0$ otherwise.

Denote by ϕ a GNN model that maps a graph to a probability distribution over a set of classes denoted by \mathcal{C} . Let \mathcal{D} denote the set of graphs that are used to train the GNN model ϕ . We focus on GNNs that adopt piecewise linear activation functions, such as MaxOut [14] and the family of ReLU [13, 15, 29].

The robust counterfactual explanation problem is defined as follows.

Definition 1 (Robust Counterfactual Explanation Problem) *Given a GNN model ϕ trained on a set of graphs \mathcal{D} , for an input graph $G = \{V, E\}$, our goal is to explain why G is predicted by the GNN model as $\phi(G)$ by identifying a small subset of edges $S \subseteq E$, such that (1) removing the set of edges in S from G that causes the maximum drop in the confidence of the original prediction; and (2) S is stable and doesn’t change when the edges and the feature representations of the nodes of G are perturbed by random noise.*

In the definition, the first requirement requires that the explanation S is counterfactual, and the second requirement requires that the explanation is robust to noisy changes on the edges and nodes of G .

4 Method

In this section, we first introduce how to extract the common decision logic of a GNN on a large set of graphs with the same predicted class. This is achieved by a decision region induced by a set of linear decision boundaries of the GNN. Then, based on the linear boundaries of the decision region, we propose a novel loss function to train a neural network that produces robust counterfactual explanations. Last, we discuss the time complexity of our method when generating explanations.

4.1 Modelling Decision Regions

Following the routines of many deep neural network explanation methods [33, 48], we extract the decision region of a GNN in the d -dimensional output space \mathbb{O}^d of the last convolution layer of the GNN. The features generated by the last convolution layer are more conceptually meaningful and more robust to noise than those raw features of input graphs, such as vertices and edges [52, 2]. Denote by ϕ_{gc} the mapping function realized by the graph convolution layers that maps an input graph G to its graph embedding $\phi_{gc}(G) \in \mathbb{O}^d$, and by ϕ_{fc} the mapping function realized by the fully connected layers that maps the graph embedding $\phi_{gc}(G)$ to a predicted distribution over the classes in C . The overall prediction $\phi(G)$ made by the GNN can be written as $\phi(G) = \phi_{fc}(\phi_{gc}(G))$.

For the GNNs that adopt piecewise linear activation functions for the hidden neurons, such as MaxOut [14] and the family of ReLU [13, 15, 29], the decision logic of ϕ_{fc} in the space \mathbb{O}^d is characterized by a piecewise linear decision boundary formed by connected pieces of decision hyperplanes in \mathbb{O}^d [1]. We call these hyperplanes **linear decision boundaries (LDBs)**, and denote by \mathcal{H} the set of LDBs induced by ϕ_{fc} . The set of LDBs in \mathcal{H} partitions the space \mathbb{O}^d into a large number of convex polytopes. A convex polytope is formed by a subset of LDBs in \mathcal{H} . All the graphs whose graph embeddings are contained in the same convex polytope are predicted as the same class [4]. Therefore, the LDBs of a convex polytope encode the common decision logic of ϕ_{fc} on all the graphs whose graph embeddings lie within the convex polytope [4]. Here, a graph G is **covered** by a convex polytope if the graph embedding $\phi_{gc}(G)$ is contained in the convex polytope.

Based on the above insight, we model the **decision region** for a set of graph instances as a convex polytope that satisfies the following two properties. First, the decision region should be induced by a subset of the LDBs in \mathcal{H} . In this way, when we extract counterfactual explanations from the LDBs, the explanations are loyal to the real decision logic of the GNN. Second, the decision region should cover many graph instances in the training dataset D , and all the covered graphs should be predicted as the same class. In this way, the LDBs of the decision region capture the common decision logic on all the graphs covered by the decision region. Here, the requirement of covering a larger number of graphs ensures that the common decision logic is general, and thus it is less likely to overfit the noise of an individual graph instance. As a result, the counterfactual explanations extracted from the LDBs of the decision region are insensitive to slight changes in the input graphs. Our method can be easily generalized to incorporate prediction confidence in the coverage measure, such as considering the count of graphs weighted by prediction confidence. To keep our discussion simple, we do not pursue this detail further in the paper.

Next, we illustrate how to extract a decision region satisfying the above two requirements. The key idea is to find a convex polytope covering a large set of graph instances in D that are predicted as the same class $c \in C$.

Denote by $D_c \subseteq D$ the set of graphs in D predicted as a class $c \in C$, by $\mathcal{P} \subseteq \mathcal{H}$ a set of LDBs that partition the space \mathbb{O}^d into a set of convex polytopes, and by $r(\mathcal{P}, c)$ the convex polytope induced by \mathcal{P} that covers the largest number of graphs in D_c . Denote by $g(\mathcal{P}, c)$ the number of graphs in D_c covered by $r(\mathcal{P}, c)$, and by $h(\mathcal{P}, c)$ the number of graphs in D that are covered by $r(\mathcal{P}, c)$ but are not predicted as class c . We extract a decision region covering a large set of graph instances in D_c by solving the following constrained optimization problem.

$$\max_{\mathcal{P} \subseteq \mathcal{H}} g(\mathcal{P}, c), \text{ s.t. } h(\mathcal{P}, c) = 0 \quad (1)$$

This formulation realizes the two properties of decision regions because $\mathcal{P} \subseteq \mathcal{H}$ ensures that the decision region is induced by a subset of LDBs in \mathcal{H} , maximizing $g(\mathcal{P}, c)$ requires that $r(\mathcal{P}, c)$ covers

a large number of graphs in D_c , and the constraint $h(\mathcal{P}, c) = 0$ ensures that all the graphs covered by $r(\mathcal{P}, c)$ are predicted as the same class c .

Once we find a solution \mathcal{P} to the above problem, the decision region $r(\mathcal{P}, c)$ can be easily obtained by first counting the number of graphs in D_c covered by each convex polytope induced by \mathcal{P} , and then select the convex polytope that covers the largest number of graphs in D_c .

4.2 Extracting Decision Regions

The optimization problem in Equation (1) is intractable for standard GNNs, mainly because it is impractical to compute \mathcal{H} , all the LDBs of a GNN. The number of LDBs in \mathcal{H} of a GNN is exponential with respect to the number of neurons in the worst case [27]. To address this challenge, we substitute \mathcal{H} by a sample $\tilde{\mathcal{H}}$ of LDBs from \mathcal{H} .

A LDB in the space \mathbb{O}^d can be written as $\mathbf{w}^\top \mathbf{x} + b = 0$, where $\mathbf{x} \in \mathbb{O}^d$ is a variable, \mathbf{w} is the basis term, and b corresponds to the bias. Following [4], for any input graph G , a linear boundary can be sampled from \mathcal{H} by computing

$$\mathbf{w} = \frac{\partial (\max_1(\phi_{fc}(\boldsymbol{\alpha})) - \max_2(\phi_{fc}(\boldsymbol{\alpha})))}{\partial \boldsymbol{\alpha}} \Big|_{\boldsymbol{\alpha}=\phi_{gc}(G)}, \quad (2)$$

and

$$b = \max_1(\phi_{fc}(\boldsymbol{\alpha})) - \max_2(\phi_{fc}(\boldsymbol{\alpha})) - \mathbf{w}^\top \boldsymbol{\alpha} \Big|_{\boldsymbol{\alpha}=\phi_{gc}(G)}, \quad (3)$$

where $\max_1(\phi_{fc}(\boldsymbol{\alpha}))$ and $\max_2(\phi_{fc}(\boldsymbol{\alpha}))$ are the largest and the second largest values in the vector $\phi_{fc}(\boldsymbol{\alpha})$, respectively. Given an input graph G , Equations (2) and (3) identify one LDB from \mathcal{H} . Thus, we can sample a subset of input graphs uniformly from D , and use Equations (2) and (3) to derive a sample of LDBs as $\tilde{\mathcal{H}} \subset \mathcal{H}$.

Now, we substitute \mathcal{H} in Equation (1) by $\tilde{\mathcal{H}}$ to produce the following problem.

$$\max_{\mathcal{P} \subseteq \tilde{\mathcal{H}}} g(\mathcal{P}, c), \text{ s.t. } h(\mathcal{P}, c) \leq \delta, \quad (4)$$

where $\delta \geq 0$ is a tolerance parameter to keep this problem feasible. The parameter δ is required because substituting \mathcal{H} by $\tilde{\mathcal{H}}$ ignores the LDBs in $\mathcal{H} \setminus \tilde{\mathcal{H}}$. Thus, the convex polytope $r(\mathcal{P}, c)$ induced by subset of boundaries in $\tilde{\mathcal{H}}$ may contain instances that are not predicted as class c . We directly set $\delta = h(\tilde{\mathcal{H}}, c)$, which is the smallest value of δ that keeps the practical problem feasible.

The problem in Equation (4) can be proven to be a Submodular Cost Submodular Cover (SCSC) problem [18] (see Appendix D for proof) that is well known to be NP-hard [5]. We adopt a greedy boundary selection method to find a good solution to this problem [40]. Specifically, we initialize \mathcal{P} as an empty set, and then iteratively select a new boundary h from $\tilde{\mathcal{H}}$ by

$$h = \arg \min_{h \in \tilde{\mathcal{H}} \setminus \mathcal{P}} \frac{g(\mathcal{P}, c) - g(\mathcal{P} \cup \{h\}, c) + \epsilon}{h(\mathcal{P}, c) - h(\mathcal{P} \cup \{h\}, c)}, \quad (5)$$

where $g(\mathcal{P}, c) - g(\mathcal{P} \cup \{h\}, c)$ is the decrease of $g(\mathcal{P}, c)$ when adding h into \mathcal{P} , and $h(\mathcal{P}, c) - h(\mathcal{P} \cup \{h\}, c)$ is the decrease of $h(\mathcal{P}, c)$ when adding h into \mathcal{P} . Both $g(\mathcal{P}, c)$ and $h(\mathcal{P}, c)$ are non-increasing when adding $h \in \tilde{\mathcal{H}}$ into \mathcal{P} because adding a new boundary h may only exclude some graphs from the convex polytope $r(\mathcal{P}, c)$.

Intuitively, in each iteration, Equation (5) selects a boundary $h \in \tilde{\mathcal{H}}$ such that adding h into \mathcal{P} reduces $g(\mathcal{P}, c)$ the least and reduces $h(\mathcal{P}, c)$ the most. In this way, we can quickly reduce $h(\mathcal{P}, c)$ to be smaller than δ without decreasing $g(\mathcal{P}, c)$ too much, which produces a good feasible solution to the practical problem. We add a small constant ϵ to the numerator such that, when there are multiple candidates of h that do not decrease $g(\mathcal{P}, c)$, we can still select the h that reduces $h(\mathcal{P}, c)$ the most.

We apply a peeling-off strategy to iteratively extract multiple decision regions. For each class $c \in C$, we first solve the practical problem once to find a decision region $r(\mathcal{P}, c)$, then we remove the graphs covered by $r(\mathcal{P}, c)$ from D_c . If there are remaining graphs predicted as the class c , we continue finding the decision regions using the remaining graphs until all the graphs in D_c are removed. When all the graphs in D_c are removed for each class $c \in C$, we stop the iteration and return the set of decision regions we found.

4.3 Producing Explanations

In this section, we introduce how to use the LDBs of decision regions to train a neural network that produces a robust counterfactual explanation as a small subset of edges of an input graph. We form explanations as a subset of edges because GNNs make decisions by aggregating messages passed on edges. Using edges instead of vertices as explanations can provide better insights on the decision logic of GNNs.

4.3.1 The Neural Network Model

Denote by f_θ the neural network to generate a subset of edges of an input graph G as the robust counterfactual explanation on the prediction $\phi(G)$. θ represents the set of parameters of the neural network. For experiments, our explanation network f consists of 2 fully connected layers with a ReLU activation and the hidden dimension of 64.

For any two connected vertices v_i and v_j of G , denote by \mathbf{z}_i and \mathbf{z}_j the embeddings produced by the last convolution layer of the GNN for the two vertices, respectively. The neural network f_θ takes \mathbf{z}_i and \mathbf{z}_j as the input and outputs the probability for the edge between v_i and v_j to be part of the explanation. This can be written as

$$\mathbf{M}_{ij} = f_\theta(\mathbf{z}_i, \mathbf{z}_j), \quad (6)$$

where \mathbf{M}_{ij} denotes the probability that the edge between v_i and v_j is contained in the explanation. When there is no edge between v_i and v_j , that is, $\mathbf{A}_{ij} = 0$, we set $\mathbf{M}_{ij} = 0$.

For an input graph $G = \{V, E\}$ with n vertices and a trained neural network f_θ , \mathbf{M} is an n -by- n matrix that carries the complete information to generate a robust counterfactual explanation as a subset of edges, denoted by $S \subseteq E$. Concretely, we obtain S by selecting all the edges in E whose corresponding entries in \mathbf{M} are larger than 0.5.

4.3.2 Training Model f_θ

For an input graph $G = (V, E)$, denote by $S \subseteq E$ the subset of edges produced by f_θ to explain the prediction $\phi(G)$, our goal is to train a good model f_θ such that the prediction on the subgraph G_S induced by S from G is consistent with $\phi(G)$; and deleting the edges in S from G produces a remainder subgraph $G_{E \setminus S}$ such that the prediction on $G_{E \setminus S}$ changes significantly from $\phi(G)$.

Since producing S by f_θ is a discrete operation that is hard to incorporate in an end-to-end training process, we define two proxy graphs to approximate G_S and $G_{E \setminus S}$, respectively, such that the proxy graphs are determined by θ through continuous functions that can be smoothly incorporated into an end-to-end training process.

The proxy graph of G_S , denoted by G_θ , is defined by regarding \mathbf{M} instead of \mathbf{A} as the adjacency matrix. That is, G_θ has exactly the same graph structure as G , but the edge weights of G_θ is given by the entries in \mathbf{M} instead of \mathbf{A} . Here, the subscript θ means G_θ is determined by θ .

The proxy graph of $G_{E \setminus S}$, denoted by G'_θ , also have the same graph structure as G , but the edge weight between each pair of vertices v_i and v_j is defined as

$$\mathbf{M}'_{ij} = \begin{cases} 1 - \mathbf{M}_{ij} & \text{if } \mathbf{A}_{ij} = 1 \\ 0 & \text{if } \mathbf{A}_{ij} = 0 \end{cases} \quad (7)$$

The edge weights of both G_θ and G'_θ are determined by θ through continuous functions, thus we can smoothly incorporate G_θ and G'_θ into an end-to-end training framework.

As discussed later in this section, we use a regularization term to force the value of each entry in \mathbf{M}_{ij} to be close to either 0 or 1, such that G_θ and G'_θ better approximate G_S and $G_{E \setminus S}$ respectively.

We formulate our loss function as

$$\mathcal{L}(\theta) = \sum_{G \in D} \{ \lambda \mathcal{L}_{same}(\theta, G) + (1 - \lambda) \mathcal{L}_{opp}(\theta, G) + \beta \mathcal{R}_{sparse}(\theta, G) + \mu \mathcal{R}_{discrete}(\theta, G) \}, \quad (8)$$

where $\lambda \in [0, 1]$, $\beta \geq 0$ and $\mu \geq 0$ are the hyperparameters controlling the importance of each term. The influence of these parameters is discussed in Appendix G. The first term of our loss function requires that the prediction of the GNN on G_θ is consistent with the prediction on G . Intuitively, this

means that the edges with larger weights in G_θ dominate the prediction on G . We formulate this term by requiring G_θ to be covered by the same decision region covering G .

Denote by \mathcal{H}_G the set of LDBs that induce the decision region covering G , and by $|\mathcal{H}_G|$ the number of LDBs in \mathcal{H}_G . For the i -th LDB $h_i \in \mathcal{H}_G$, denote by $\mathcal{B}_i(\mathbf{x}) = \mathbf{w}_i^\top \mathbf{x} + b_i$, where \mathbf{w}_i and b_i are the basis and bias of h_i , respectively, and $\mathbf{x} \in \mathbb{O}^d$ is a point in the space \mathbb{O}^d . The sign of $\mathcal{B}_i(\mathbf{x})$ indicates whether a point \mathbf{x} lies on the positive side or the negative side of h_i , and the absolute value $|\mathcal{B}_i(\mathbf{x})|$ is proportional to the distance of a point \mathbf{x} from h_i . Denote by $\sigma(\cdot)$ the standard sigmoid function, we formulate the first term of our loss function as

$$\mathcal{L}_{same}(\theta, G) = \frac{1}{|\mathcal{H}_G|} \sum_{h_i \in \mathcal{H}_G} \sigma(-\mathcal{B}_i(\phi_{gc}(G)) * \mathcal{B}_i(\phi_{gc}(G_\theta))), \quad (9)$$

such that minimizing $\mathcal{L}_{same}(\theta, G)$ encourages the graph embeddings $\phi_{gc}(G)$ and $\phi_{gc}(G_\theta)$ to lie on the same side of every LDB in \mathcal{H}_G . Thus, G_θ is encouraged to be covered by the same decision region covering G .

The second term of our loss function optimizes the counterfactual property of the explanations by requiring the prediction on G'_θ to be significantly different from the prediction on G . Intuitively, this means that the set of edges with larger weights in G_θ are good counterfactual explanations because reducing the weights of these edges significantly changes the prediction. Following the above intuition, we formulate the second term as

$$\mathcal{L}_{opp}(\theta, G) = \min_{h_i \in \mathcal{H}_G} \sigma(\mathcal{B}_i(\phi_{gc}(G)) * \mathcal{B}_i(\phi_{gc}(G'_\theta))), \quad (10)$$

such that minimizing $\mathcal{L}_{opp}(\theta, G)$ encourages the graph embeddings $\phi_{gc}(G)$ and $\phi_{gc}(G'_\theta)$ to lie on the opposite sides of at least one LDB in \mathcal{H}_G . This further means that G'_θ is encouraged not to be covered by the decision region covering G , thus the prediction on G'_θ can be changed significantly from the prediction on G .

Similar to [45], we use a L1 regularization $\mathcal{R}_{sparse}(\theta, G) = \|\mathbf{M}\|_1$ on the matrix \mathbf{M} produced by f_θ on an input graph G to produce a sparse matrix \mathbf{M} , such that only a small number of edges in G are selected as the counterfactual explanation. We also follow [45] to use an entropy regularization

$$\mathcal{R}_{discrete}(\theta, G) = -\frac{1}{|\mathbf{M}|} \sum_{i,j} (\mathbf{M}_{ij} \log(\mathbf{M}_{ij}) + (1 - \mathbf{M}_{ij}) \log(1 - \mathbf{M}_{ij})) \quad (11)$$

to push the value of each entry in \mathbf{M}_{ij} to be close to either 0 or 1, such that G_θ and G'_θ approximate G_S and $G_{E \setminus S}$ well, respectively.

Now we can use the graphs in D and the extracted decision regions to train the neural network f_θ in an end-to-end manner by minimizing $\mathcal{L}(\theta)$ over θ using back propagation. Once we finish training f_θ , we can first apply f_θ to produce the matrix \mathbf{M} for an input graph $G = (V, E)$, and then obtain the explanation S by selecting all the edges in E whose corresponding entries in \mathbf{M} are larger than 0.5. We do not need the extracted boundaries for inference as the the decision logic of GNN is already distilled into the explanation network f during the training.

As discussed in Appendix B, our method can be easily extended to generate robust counterfactual explanations for node classification tasks.

Our method is highly efficient with a time complexity $O(|E|)$ for explaining the prediction on an input graph G , where $|E|$ is the total number of edges in G . Additionally, the neural network f_θ can be directly used without retraining to predict explanations on unseen graphs. Thus our method is significantly faster than the other methods [45, 32, 47, 38] that require retraining each time when generating explanations on a new input graph.

5 Experiments

We conduct series of experiments to compare our method with the state-of-the-art methods including GNNExplainer [45], PGExplainer [25], PGM-Explainer [38], SubgraphX [47] and CF-GNNExplainer [24]. For the methods that identify a set of vertices as an explanation, we use the set of vertices to induce a subgraph from the input graph, and then use the set of edges of the induced subgraph as the explanation. For the methods that identify a subgraph as an explanation, we directly use the set of edges of the identified subgraph as the explanation.

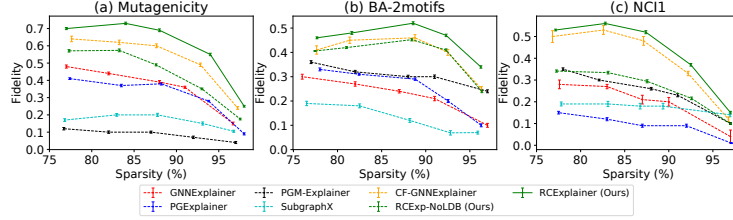


Figure 1: Fidelity performance averaged across 10 runs for the datasets at different levels of sparsity.

To demonstrate the effectiveness of the decision regions, we derive another baseline method named RCExp-NoLDB that adopts the general framework of RCExp (Ours) but does not use the LDBs of decision regions to generate explanations. Instead, RCExp-NoLDB directly maximizes the prediction confidence on class c for G_θ and minimizes the prediction confidence of class c for G'_θ .

We evaluate the explanation performance on two typical tasks: the graph classification task that uses a GNN to predict the class of an input graph, and the node classification task that uses a GNN to predict the class of a graph node. For the graph classification task, we use one synthetic dataset, BA-2motifs [25], and two real-world datasets, Mutagenicity [21] and NCI1 [39]. For the node classification task, we use the same four synthetic datasets as used by GNNExplainer [45], namely, BA-SHAPES, BA-COMMUNITY, TREE-CYCLES and TREE-GRID.

Limited by space, we only report here the key results on the graph classification task for fidelity, robustness and efficiency. Please refer to Appendix E for details on datasets, baselines and the experiment setups. Detailed experimental comparison on the node classification task will be discussed in Appendix F where we show that our method produces extremely accurate explanations. The code³ is publicly available.

5.1 Fidelity

Fidelity is measured by the decrease of prediction confidence after removing the explanation (i.e., a set of edges) from the input graph [32]. We use fidelity to evaluate how counterfactual the generated explanations are on the datasets Mutagenicity, NCI1 and BA-2motifs. A large fidelity score indicates stronger counterfactual characteristics. It is important to note that fidelity may be sensitive to sparsity of explanations. The sparsity of an explanation S with respect to an input graph $G = (V, E)$ is $sparsity(S, G) = 1 - \frac{|S|}{|E|}$, that is, the percentage of edges remaining after the explanation is removed from G . We only compare explanations with the same level of sparsity.

Figure 1 shows the results about fidelity. Our approach achieves the best fidelity performance at all levels of sparsity. The results validate the effectiveness of our method in producing highly counterfactual explanations. RCExp (Ours) also significantly outperforms RCExp-NoLDB. This confirms that using LDBs of decision regions extracted from GNNs produces more faithful counterfactual explanations.

CF-GNNExplainer performs the best among the rest of the methods. This is expected as it optimizes the counterfactual behavior of the explanations which results in higher fidelity for the explanations in comparison to those produced by other methods such as GNNExplainer and PGExplainer.

The fidelity performance of SubgraphX reported in [47] was obtained by setting the features of nodes that are part of the explanation to 0 but not removing the explanation edges from the input graph. This does not remove the message passing roles of the explanation nodes from the input graph because the edges connected to those nodes still can pass messages. In our experiments, we directly block the messages that are passed on the edges in the explanation, which completely prevents the explanation nodes in the input graph to participate in the message passing. As a result, the performance of SubgraphX drops significantly.

³Code available at <https://marketplace.huaweicloud.com/markets/aihub/notebook/detail/?id=e41f63d3-e346-4891-bf6a-40e64b4a3278>

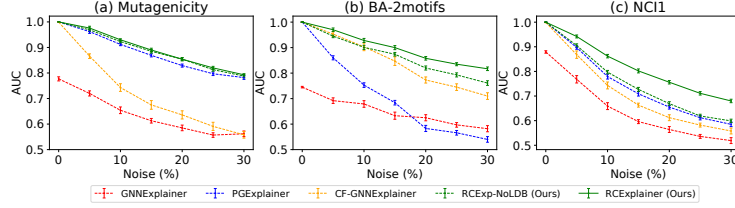


Figure 2: Noise robustness (AUC) averaged across 10 runs for the datasets at different levels of noise.

5.2 Robustness Performance

In this experiment, we evaluate the robustness of all methods by quantifying how much an explanation changes after adding noise to the input graph. For an input graph G and the explanation S , we produce a perturbed graph G' by adding random noise to the node features and randomly adding or deleting some edges of the input graph such that the prediction on G' is consistent with the prediction on G . Using the same method we obtain the explanation S' on G' . Considering top- k edges of S as the ground-truth and comparing S' against them, we compute a receiver operating characteristic (ROC) curve and evaluate the robustness by the area under curve (AUC) of the ROC curve. We report results for $k = 8$ in Figure 2. Results for other values of k are included in Appendix F where we observe similar trend.

Figure 2 shows the AUC of GNNExplainer, PGExplainer, RCExp-NoLDB and RCExplainer at different levels of noise. A higher AUC indicates better robustness. The percentage of noise shows the proportion of nodes and edges that are modified. Baselines such as PGM-Explainer and SubgraphX are not included in this experiment as they do not output the edge weights that are required for computing AUC. We present additional robustness experiments in Appendix F where we extend all the baselines to report node and edge level accuracy.

GNNExplainer performs the worst on most of the datasets, since it optimizes each graph independently without considering other graphs in the training set. Even when no noise is added, the AUC of GNNExplainer is significantly lower than 1 because different runs produce different explanations for the same graph prediction. PGExplainer is generally more robust than GNNExplainer because the neural network they trained to produce explanations implicitly considers all the graphs used for training. CF-GNNExplainer also performs worse than RCExplainer, which means it is more susceptible to the noise as compared to RCExplainer.

Our method achieves the best AUC on all the datasets, because the common decision logic carried by the decision regions of a GNN is highly robust to noise. PGExplainer achieves a comparable performance as our method on the Mutagenicity dataset, because the samples of this dataset share a lot of common structures such as carbon rings, which makes it easier for the neural network trained by PGExplainer to identify these structures in presence of noise. However, for BA-2motifs and NCI1, this is harder as samples share very few structures and thus the AUC of PGExplainer drops significantly. RCExplainer also significantly outperforms RCExp-NoLDB on these datasets which highlights the role of decision boundaries in making our method highly robust.

Method	GNNExplainer	PGExplainer	PGM-Explainer	SubgraphX	CF-GNNExplainer	RCExplainer
Time	1.2s \pm 0.2	0.01s \pm 0.03	13.1s \pm 3.9	77.8s \pm 4.5	4.6s \pm 0.2	0.01s \pm 0.02

Table 1: Average time cost for producing an explanation on a single graph sample.

Efficiency. We evaluate efficiency by comparing the average computation time taken for inference on unseen graph samples. Table 1 shows the results on the Mutagenicity dataset. Since our method also can be directly used for unseen data without any retraining, it is as efficient as PGExplainer and significantly faster than GNNExplainer, PGM-Explainer, SubgraphX and CF-GNNExplainer.

6 Conclusion

In this paper, we develop a novel method for producing counterfactual explanations on GNNs. We extract decision boundaries from the given GNN model to formulate an intuitive and effective

counterfactual loss function. We optimize this loss to train a neural network to produce explanations with strong counterfactual characteristics. Since the decision boundaries are shared by multiple samples of the same predicted class, explanations produced by our method are robust and do not overfit the noise. Our experiments on synthetic and real-life benchmark datasets strongly validate the efficacy of our method. In this work, we focus on GNNs that belong to Piecewise Linear Neural Networks (PLNNs). Extending our method to other families of GNNs and tasks such as link prediction, remains an interesting future direction.

Our method will benefit multiple fields where GNNs are intensively used. By allowing the users to interpret the predictions of complex GNNs better, it will promote transparency, trust and fairness in the society. However, there also exist some inherent risks. A generated explanation may expose private information if our method is not coupled with an adequate privacy protection technique. Also, some of the ideas presented in this paper may be adopted and extended to improve adversarial attacks. Without appropriate defense mechanisms, the misuse of such attacks poses a risk of disruption in the functionality of GNNs deployed in the real world. That said, we firmly believe that these risks can be mitigated through increased awareness and proactive measures.

Acknowledgments and Disclosure of Funding

Lingyang Chu’s research is supported in part by the startup grant provided by the Department of Computing and Software of McMaster University. All opinions, findings, conclusions, and recommendations in this paper are those of the authors and do not necessarily reflect the views of the funding agencies.

References

- [1] J. Adebayo, J. Gilmer, M. Muelly, I. Goodfellow, M. Hardt, and B. Kim. Sanity checks for saliency maps. In *Advances in Neural Information Processing Systems*, volume 31, 2018.
- [2] A. Bojchevski and S. Günnemann. Certifiable robustness to graph perturbations. *arXiv preprint arXiv:1910.14356*, 2019.
- [3] E. Cho, S. A. Myers, and J. Leskovec. Friendship and mobility: user movement in location-based social networks. In *Proceedings of the 17th ACM SIGKDD international conference on Knowledge discovery and data mining*, pages 1082–1090, 2011.
- [4] L. Chu, X. Hu, J. Hu, L. Wang, and J. Pei. Exact and consistent interpretation for piecewise linear neural networks: A closed form solution. In *Proceedings of the 24th ACM SIGKDD International Conference on Knowledge Discovery & Data Mining*, pages 1244–1253, 2018.
- [5] V. Crawford, A. Kuhnle, and M. Thai. Submodular cost submodular cover with an approximate oracle. In *International Conference on Machine Learning*, pages 1426–1435. PMLR, 2019.
- [6] A. K. Debnath, R. L. Lopez de Compadre, G. Debnath, A. J. Shusterman, and C. Hansch. Structure-activity relationship of mutagenic aromatic and heteroaromatic nitro compounds. correlation with molecular orbital energies and hydrophobicity. *Journal of medicinal chemistry*, 34(2):786–797, 1991.
- [7] M. Denil, S. G. Colmenarejo, S. Cabi, D. Saxton, and N. de Freitas. Programmable agents. *arXiv preprint arXiv:1706.06383*, 2017.
- [8] Y. Duan, M. Andrychowicz, B. C. Stadie, J. Ho, J. Schneider, I. Sutskever, P. Abbeel, and W. Zaremba. One-shot imitation learning. *arXiv preprint arXiv:1703.07326*, 2017.
- [9] W. Fan, Y. Ma, Q. Li, Y. He, E. Zhao, J. Tang, and D. Yin. Graph neural networks for social recommendation. In *The World Wide Web Conference*, pages 417–426, 2019.
- [10] T. Freiesleben. Counterfactual explanations & adversarial examples—common grounds, essential differences, and potential transfers. *arXiv preprint arXiv:2009.05487*, 2020.
- [11] A. Ghorbani, A. Abid, and J. Zou. Interpretation of neural networks is fragile. In *Proceedings of the AAAI Conference on Artificial Intelligence*, volume 33, pages 3681–3688, 2019.
- [12] X. Glorot and Y. Bengio. Understanding the difficulty of training deep feedforward neural networks. In *Proceedings of the thirteenth international conference on artificial intelligence and statistics*, pages 249–256. JMLR Workshop and Conference Proceedings, 2010.

- [13] X. Glorot, A. Bordes, and Y. Bengio. Deep sparse rectifier neural networks. In *Proceedings of the fourteenth international conference on artificial intelligence and statistics*, pages 315–323. JMLR Workshop and Conference Proceedings, 2011.
- [14] I. Goodfellow, D. Warde-Farley, M. Mirza, A. Courville, and Y. Bengio. Maxout networks. In *International conference on machine learning*, pages 1319–1327. PMLR, 2013.
- [15] K. He, X. Zhang, S. Ren, and J. Sun. Delving deep into rectifiers: Surpassing human-level performance on imagenet classification. In *Proceedings of the IEEE international conference on computer vision*, pages 1026–1034, 2015.
- [16] L. Holdijk, M. Boon, S. Henckens, and L. de Jong. [re] parameterized explainer for graph neural network. In *ML Reproducibility Challenge 2020*, 2021.
- [17] W. Huber, V. J. Carey, L. Long, S. Falcon, and R. Gentleman. Graphs in molecular biology. *BMC bioinformatics*, 8(6):1–14, 2007.
- [18] R. K. Iyer and J. A. Bilmes. Submodular optimization with submodular cover and submodular knapsack constraints. In *Advances in Neural Information Processing Systems*, volume 26, 2013.
- [19] M. Jiang, Z. Li, S. Zhang, S. Wang, X. Wang, Q. Yuan, and Z. Wei. Drug–target affinity prediction using graph neural network and contact maps. *RSC Advances*, 10(35):20701–20712, 2020.
- [20] H. Jin and X. Zhang. Latent adversarial training of graph convolution networks. In *ICML Workshop on Learning and Reasoning with Graph-Structured Representations*, 2019.
- [21] J. Kazius, R. McGuire, and R. Bursi. Derivation and validation of toxicophores for mutagenicity prediction. *Journal of medicinal chemistry*, 48(1):312–320, 2005.
- [22] T. N. Kipf and M. Welling. Semi-supervised classification with graph convolutional networks. In *5th International Conference on Learning Representations, ICLR 2017, Conference Track Proceedings*, 2017.
- [23] M. Liu, Y. Luo, L. Wang, Y. Xie, H. Yuan, S. Gui, H. Yu, Z. Xu, J. Zhang, Y. Liu, K. Yan, H. Liu, C. Fu, B. Oztekin, X. Zhang, and S. Ji. DIG: A turnkey library for diving into graph deep learning research. *arXiv preprint arXiv:2103.12608*, 2021.
- [24] A. Lucic, M. ter Hoeve, G. Tolomei, M. de Rijke, and F. Silvestri. Cf-gnnexplainer: Counterfactual explanations for graph neural networks. *arXiv preprint arXiv:2102.03322*, 2021.
- [25] D. Luo, W. Cheng, D. Xu, W. Yu, B. Zong, H. Chen, and X. Zhang. Parameterized explainer for graph neural network. In *Advances in Neural Information Processing Systems*, volume 33, pages 19620–19631, 2020.
- [26] C. Molnar. *Interpretable Machine Learning*. 2019. <https://christophm.github.io/interpretable-ml-book/>.
- [27] G. Montúfar, R. Pascanu, K. Cho, and Y. Bengio. On the number of linear regions of deep neural networks. *arXiv preprint arXiv:1402.1869*, 2014.
- [28] R. Moraffah, M. Karami, R. Guo, A. Raglin, and H. Liu. Causal interpretability for machine learning-problems, methods and evaluation. *ACM SIGKDD Explorations Newsletter*, 22(1):18–33, 2020.
- [29] V. Nair and G. E. Hinton. Rectified linear units improve restricted boltzmann machines. In *Icml*, 2010.
- [30] D. Numeroso and D. Bacciu. Meg: Generating molecular counterfactual explanations for deep graph networks. *arXiv preprint arXiv:2104.08060*, 2021.
- [31] D. E. Pires, T. L. Blundell, and D. B. Ascher. pkcsm: predicting small-molecule pharmacokinetic and toxicity properties using graph-based signatures. *Journal of medicinal chemistry*, 58(9):4066–4072, 2015.
- [32] P. E. Pope, S. Kolouri, M. Rostami, C. E. Martin, and H. Hoffmann. Explainability methods for graph convolutional neural networks. In *Proceedings of the IEEE/CVF Conference on Computer Vision and Pattern Recognition*, pages 10772–10781, 2019.
- [33] R. R. Selvaraju, M. Cogswell, A. Das, R. Vedantam, D. Parikh, and D. Batra. Grad-cam: Visual explanations from deep networks via gradient-based localization. In *Proceedings of the IEEE international conference on computer vision*, pages 618–626, 2017.
- [34] P. L. Simon, M. Taylor, and I. Z. Kiss. Exact epidemic models on graphs using graph-automorphism driven lumping. *Journal of mathematical biology*, 62(4):479–508, 2011.

- [35] K. Simonyan, A. Vedaldi, and A. Zisserman. Deep inside convolutional networks: Visualising image classification models and saliency maps. *ICLR*, 2014.
- [36] K. Sokol and P. A. Flach. Counterfactual explanations of machine learning predictions: opportunities and challenges for ai safety. In *SafeAI@ AAAI*, 2019.
- [37] P. Velickovic, G. Cucurull, A. Casanova, A. Romero, P. Liò, and Y. Bengio. Graph attention networks. In *6th International Conference on Learning Representations, ICLR 2018, Conference Track Proceedings*, 2018.
- [38] M. Vu and M. T. Thai. Pgm-explainer: Probabilistic graphical model explanations for graph neural networks. In *Advances in Neural Information Processing Systems*, volume 33, pages 12225–12235, 2020.
- [39] N. Wale and G. Karypis. Comparison of descriptor spaces for chemical compound retrieval and classification. In *Sixth International Conference on Data Mining (ICDM’06)*, pages 678–689, 2006. doi: 10.1109/ICDM.2006.39.
- [40] L. A. Wolsey. An analysis of the greedy algorithm for the submodular set covering problem. *Combinatorica*, 2(4):385–393, 1982.
- [41] J. Xiong, Z. Xiong, K. Chen, H. Jiang, and M. Zheng. Graph neural networks for automated de novo drug design. *Drug Discovery Today*, 2021.
- [42] H. Xu, Y. Ma, H.-C. Liu, D. Deb, H. Liu, J.-L. Tang, and A. K. Jain. Adversarial attacks and defenses in images, graphs and text: A review. *International Journal of Automation and Computing*, 17(2):151–178, 2020.
- [43] K. Xu, H. Chen, S. Liu, P.-Y. Chen, T.-W. Weng, M. Hong, and X. Lin. Topology attack and defense for graph neural networks: An optimization perspective. *arXiv preprint arXiv:1906.04214*, 2019.
- [44] R. Yin, K. Li, G. Zhang, and J. Lu. A deeper graph neural network for recommender systems. *Knowledge-Based Systems*, 185:105020, 2019.
- [45] Z. Ying, D. Bourgeois, J. You, M. Zitnik, and J. Leskovec. Gnnexplainer: Generating explanations for graph neural networks. In *Advances in Neural Information Processing Systems*, volume 32, 2019.
- [46] H. Yuan, J. Tang, X. Hu, and S. Ji. Xggn: Towards model-level explanations of graph neural networks. In *Proceedings of the 26th ACM SIGKDD International Conference on Knowledge Discovery & Data Mining*, pages 430–438, 2020.
- [47] H. Yuan, H. Yu, J. Wang, K. Li, and S. Ji. On explainability of graph neural networks via subgraph explorations. *arXiv preprint arXiv:2102.05152*, 2021.
- [48] M. D. Zeiler and R. Fergus. Visualizing and understanding convolutional networks. In *European conference on computer vision*, pages 818–833. Springer, 2014.
- [49] J. Zhang, S. A. Bargal, Z. Lin, J. Brandt, X. Shen, and S. Sclaroff. Top-down neural attention by excitation backprop. *International Journal of Computer Vision*, 126(10):1084–1102, 2018.
- [50] M. Zhang and Y. Chen. Link prediction based on graph neural networks. In *Advances in Neural Information Processing Systems*, volume 31, 2018.
- [51] D. Zügner and S. Günnemann. Adversarial attacks on graph neural networks via meta learning. *arXiv preprint arXiv:1902.08412*, 2019.
- [52] D. Zügner and S. Günnemann. Certifiable robustness and robust training for graph convolutional networks. In *Proceedings of the 25th ACM SIGKDD International Conference on Knowledge Discovery & Data Mining*, pages 246–256, 2019.
- [53] D. Zügner, A. Akbarnejad, and S. Günnemann. Adversarial attacks on neural networks for graph data. In *Proceedings of the 24th ACM SIGKDD International Conference on Knowledge Discovery & Data Mining*, pages 2847–2856, 2018.

A Illustration of RCExplainer’s training

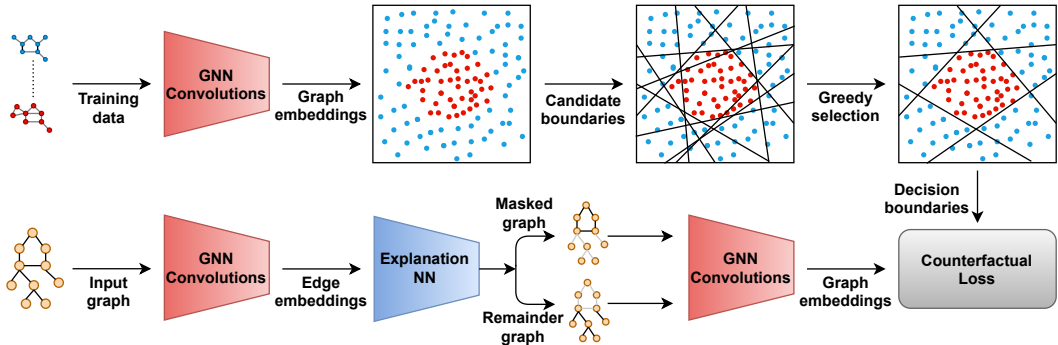


Figure 3: For training of RCExplainer, decision boundaries are extracted from the feature space of graph embeddings after the last graph convolution layer. After processing, a subset of boundaries is obtained and used to train an explanation neural network that takes edge activations from the convolution layers of GNN as input and predicts a mask over the adjacency matrix for the given graph sample. Counterfactual loss is used to optimize the explanation network.

B Node classification

Our method is directly applicable to the task of node classification with few simple modifications. Instead of extracting Linear Decision Boundaries (LDBs) in feature space of graph embeddings, we operate on the feature space of node embeddings obtained after the last graph convolution layer. We use the greedy method described in Equation (5) to find the decision regions for each class, except for the node classification, the functions $g(\cdot)$ and $h(\cdot)$ denote the coverage of nodes rather than graphs.

The next step to train the explanation network f_θ to generate counterfactual explanations for node classification is identical to the procedure described in Section 4 except for one difference. For node classification, since a node’s prediction is only influenced by its local neighborhood, therefore we only need to consider the computation graph of the given node while generating the explanation. The computation graph of a node is defined as k -hop neighborhood of the node, where k refers to number of graph convolution layers in the given GNN model ϕ . In other words, GNN performs k steps of message passing through its graph convolution layers during the forward pass to effectively convolve k -hop neighborhood of the given node. Hence, the output of f_θ is the output mask over the adjacency matrix of the computation graph of the given node. The edges with mask values more than 0.5 are chosen from the computation subgraph to form the explanation subset S that can explain the original node classification prediction.

C Interpreting individual boundaries

We present a case study to demonstrate that our method can be adapted to answer the question, “Which substructures make the samples of one class different from the samples of other specific class, and therefore can be masked to flip the prediction between the two given classes?”. This is useful in various fields, for instance, in drug discovery where the classes correspond to different chemical properties possible of a drug compound, researchers are often interested in understanding the role of chemical structures that result in a prediction of a particular property instead of another specific one. Also, this is especially helpful for debugging in cases where one expects a particular output for the given input but the GNN’s prediction does not agree with the expectation.

This case corresponds to a more constrained setting of counterfactual explanations as the target prediction is also predetermined. Let the original predicted label and the target label on a given graph G be denoted by c_i and c_j respectively. Since our method explicitly models the boundaries separating the samples of one class from the samples of other classes, our method can be easily adapted to answer such questions. If we are able to only interpret the boundary separating the samples of the given two classes, this would allow us to uncover the substructures that make the samples of first

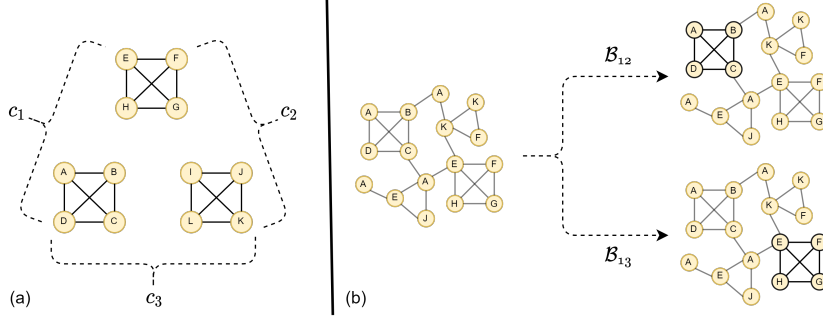


Figure 4: (a) Three classes and the motifs associated with each class are shown. All samples of the same class contain same two motifs. (b) Explanation results for an instance of class c_1 are shown w.r.t both of the boundaries separately. In both cases, RCExplainer correctly identifies the motif (highlighted in black) that is associated with the class c_1 but not associated with the class that lies on the other side of the given boundary.

class different from the samples of the other class. To address this, we modify the loss terms to

$$\mathcal{L}_{same}(\theta, G) = \sigma(-\mathcal{B}_{ij}(\phi_{gc}(G)) * \mathcal{B}_{ij}(\phi_{gc}(G_\theta))), \quad (12)$$

$$\mathcal{L}_{opp}(\theta, G) = \sigma(\mathcal{B}_{ij}(\phi_{gc}(G)) * \mathcal{B}_{ij}(\phi_{gc}(G'_\theta))), \quad (13)$$

where \mathcal{B}_{ij} refers to the specific boundary in the set \mathcal{P} separating the samples with predicted label c_i from the samples with the predicted label c_j . Since we are only concerned about changing the outcome from c_i to c_j , we need to consider only the boundary separating these classes while formulating the loss for the network.

We verify this on a synthetic graph classification dataset with 3 classes, c_1 , c_2 and c_3 such that each graph sample contains exactly 2 motifs. Both the motifs jointly determine the class because each possible pair of classes share exactly one motif as shown in Figure 4(a). We show explanation results produced by RCExplainer on an instance of class c_1 in Figure 4(b). For a given graph sample of class c_1 , we separately find explanations with respect to each of the two boundaries \mathcal{B}_{12} and \mathcal{B}_{13} . \mathcal{B}_{12} separates c_1 from c_2 , while \mathcal{B}_{13} separates c_1 from c_3 . We can see in the Figure 4(b) that optimizing our method w.r.t \mathcal{B}_{12} correctly identifies the motif (ABCD) in the sample that is not associated with the class c_2 . The other motif (EFGH) which is also associated with the c_2 is not considered important by the method. When we find the explanation for the same graph sample but with respect to the boundary \mathcal{B}_{13} , the results are opposite and align with the expectations. In this case, the motif (EFGH) that is not associated with c_3 is highlighted instead of the motif (ABCD). We observe similar behavior on the instances of other classes where interpreting an instance with respect to a single boundary correctly identifies the motif that identifies the given class from the other class.

In conclusion, the above case study demonstrates that our method can highlight the motif unique to the class c_i by interpreting the boundary \mathcal{B}_{ij} separating the classes c_i and c_j . Removing the highlighted motif from the given sample causes the drop in confidence of original predicted label c_i while increasing the confidence for the class c_j .

D Proof: Decision region extraction is an instance of SCSC optimization

Now we prove that the optimization problem in Equation (4) is an instance of Submodular Cover Submodular Cost (SCSC) problem.

The Equation (4) can be written as

$$\min_{\mathcal{P} \subseteq \mathcal{H}} D_c - g(\mathcal{P}, c), \text{ s.t. } D'_c - h(\mathcal{P}, c) \geq D'_c - \delta. \quad (14)$$

Maximizing $g(\mathcal{P}, c)$ denotes maximizing the coverage of the set of boundaries \mathcal{P} for the samples of class c denoted by D_c . This can be seen as minimizing $D_c - g(\mathcal{P}, c)$ which denotes the number of

graph samples of class c that are not covered by $g(\mathcal{P}, c)$ and thus exclusive to D_c . D'_c in the constraint is equal to $D - D_c$ that denotes the set of graph samples in the dataset D that do not belong to the class c .

Let us denote $D_c - g(\mathcal{P}, c)$ by function $g'(\mathcal{P})$ and $D'_c - h(\mathcal{P}, c)$ by $h'(\mathcal{P})$. To prove that the optimization problem in Equation (14) is an instance of SCSC problem, we prove the functions $g'(\mathcal{P})$ and $h'(\mathcal{P})$ are submodular with respect to \mathcal{P} .

For function $g'(\mathcal{P})$ to be submodular with respect to \mathcal{P} , we show that for any two arbitrary sets of LDBs denoted by $\mathcal{P} \subseteq \tilde{\mathcal{H}}$ and $\mathcal{Q} \subseteq \tilde{\mathcal{H}}$, if $\mathcal{P} \subseteq \mathcal{Q}$ then

$$g'(\mathcal{P} + \{h\}) - g'(\mathcal{P}) \geq g'(\mathcal{Q} + \{h\}) - g'(\mathcal{Q}) \quad (15)$$

is always satisfied for a linear decision boundary $h \in \tilde{\mathcal{H}} \setminus \mathcal{Q}$.

As discussed in Section 4 the LDBs in \mathcal{P} induce a convex polytope $r(\mathcal{P}, c)$ that has the maximum coverage of samples of class c . Adding a new boundary h to \mathcal{P} may remove (separate) some samples of class c from $r(\mathcal{P}, c)$ and lower its coverage. This reduction in coverage is denoted by the term $g'(\mathcal{P} + \{h\}) - g'(\mathcal{P})$ on the left hand side of Equation (15). Similarly the term $g'(\mathcal{Q} + \{h\}) - g'(\mathcal{Q})$ on the right hand side of Equation (15) denotes the reduction in coverage for the subset \mathcal{Q} .

Now, since $\mathcal{P} \subseteq \mathcal{Q}$, the set of graph samples contained in the polytope $r(\mathcal{Q}, c)$ is subset of the graph samples contained in the polytope $r(\mathcal{P}, c)$. Hence, adding new a LDB h to \mathcal{P} is not going to remove less number of samples from the polytope $r(\mathcal{P}, c)$ as compared to the samples removed from the polytope $r(\mathcal{Q}, c)$. Therefore, the function $g'(\mathcal{P})$ is submodular with respect to \mathcal{P} .

Similarly, we can prove the function $h'(\mathcal{P})$ to be submodular with respect to \mathcal{P} . This concludes the proof.

E Implementation details

Datasets. Table 2 shows the properties of all the datasets used in experiments. The last row corresponds to the test accuracy of the GCN model we train on the corresponding dataset.

	BA-SHAPES	BA-COMMUNITY	TREE-CYCLES	TREE-GRID	BA-2motifs	Mutagenicity NCII	
# of Nodes (avg)	700	1400	871	1020	25	30.32	29.87
# of Edges (avg)	2050	4460	970	2540	25.48	30.77	32.30
# of Graphs	1	1	1	1	700	4337	4110
# of Classes	4	8	2	2	2	2	2
Base	BA graph	BA graph	Tree	Tree	BA graph	—	—
Motifs	House	House	Cycle	Grid	House & Cycle	—	—
License	Apache 2.0	Apache 2.0	Apache 2.0	Apache 2.0	—	—	—
Test accuracy	0.98	0.95	0.99	0.99	0.91	0.91	0.84

Table 2: Properties of the datasets used and the test accuracy of the corresponding trained GCN models.

Baselines. For the baselines, we use publically available implementations provided in [45, 16, 38, 23] to obtain the results. Implementation of GNNExplainer provided by [45] is licensed under Apache 2.0 license while implementation of SubgraphX provided by [23] is licensed under GNU General Public License v3.0. We use the default parameters provided by the authors for the baselines.

For the local baseline RCExp-NoLDB, we use same setup as RCExplainer except we don't use LDBs for training the explanation network f . The loss function denoted by \mathcal{L}_{conf} for this baseline aligns with the loss functions of GNNExplainer and PGExplainer except we introduce a second term to enforce the counterfactual characteristics. We directly maximize the confidence of the original predicted class c on the masked graph G_θ and minimize the confidence of original predicted class for the remainder graph G'_θ . \mathcal{L}_{conf} can be expressed as :

$$\mathcal{L}_{conf}(\theta, G) = -\log(P_\phi(Y = c|X = G_\theta)) - \frac{\eta}{\log(P_\phi(Y = c|X = G'_\theta))}, \quad (16)$$

where $P_\phi(Y|X = G_x)$ corresponds to the conditional probability distribution learnt by GNN model ϕ for G_x as input graph. Y corresponds to the random variable representing the set of classes \mathcal{C} and X is the random variable representing possible input graphs for the GNN ϕ . Here η is a hyperparameter that represents the weight of the second term in the loss function. The loss \mathcal{L}_{conf} is jointly minimized with the regularizers \mathcal{R}_{sparse} and $\mathcal{R}_{discrete}$ specified in Section 4.

Training details. We follow [45, 25] and use the same architecture to train a GNN model with 3 graph convolution layers for generating explanations on each dataset. Consistent with prior works [45, 25, 38], we use (80/10/10)% random split for training/validation/test for each dataset.

We use Adam optimizer to tune the parameters of f_θ and set learning rate to 0.001. We train our method for 600 epochs. For node classification datasets, we set λ to 0.85, β to 0.006 and μ to 0.66. For graph classification datasets, we set λ to 0.1, μ to 0.66. β is set to 6×10^{-5} for BA-2motifs and NCI1, and to 6×10^{-4} for Mutagenicity. We also scale the combined loss by factor of 15 for all the datasets. The number of LDBs to be sampled from GNN for each class is set to 50. Empirically, we find that this is enough as the subset of LDBs selected greedily from this set is able to cover all the samples of the given class. Our codebase is built on the top of implementations provided by [45, 25].

All of the experiments are conducted on a Linux machine with an Intel i7-8700K processor and a Nvidia GeForce GTX 1080 Ti GPU with 11GB memory. Our code is implemented using python 3.8.5 with Pytorch 1.8.1 that uses CUDA version 10.0.

F Additional experiments

Fidelity. As described in Section 5, counterfactual characteristic of an explanation is measured by using fidelity as an evaluation metric. It is defined as drop in confidence of the original predicted class after masking the produced explanation in the original graph [32]. Since, we produce explanations as edges, we mask the edges in the input graph to calculate the drop. Fidelity for the input graph G and the produced explanation S is formally written as

$$fidelity(S, G) = P_\phi(Y = c|X = G) - P_\phi(Y = c|X = G_{E \setminus S}), \quad (17)$$

where c denotes the class predicted by ϕ for G . As discussed in Section 5, explanations are mostly useful, if they are sparse (concise). Sparsity is defined as the fraction of total edges that are present in E but not in S :

$$sparsity(S, G) = 1 - \frac{|E|}{|S|}, \quad (18)$$

However, since the approaches like SubgraphX and PGM-Explainer do not report the importance ranking of edges of G , it’s not feasible to completely control the edge sparsity of the desired explanation. Hence, we take samples with similar sparsity level for comparison. Consistent with prior works [45, 25], we compute fidelity for the samples that are labelled positive, for instance in Mutagenicity dataset, we compute fidelity for the compounds that are labelled as mutagenic. The results are presented in Figure 1.

Robustness to noise.

As discussed in Section 5, we use AUC to compare robustness of different methods. AUC is defined as area under receiver operating characteristic (ROC) curve of a binary classifier. We consider the top- k edges of the produced explanation S for the input graph G as ground-truth. After we obtain the explanation S' for the noisy sample G' , we formulate this as binary classification problem. For each edge in G' , if it is present in the top- k edges of the produced explanation S , then it is labeled positive, and negative otherwise. For G' , the mask weight of an edge predicted by explanation network f_θ is the probability of the corresponding edge being classified as positive. Limited by space, we only reported the results for $k = 8$ in Section 5. Now, we report the results for $k = 4$ and $k = 12$ in Figure 5 where we observe similar trend as observed in Figure 2. RCExplainer outperforms the rest of the methods by big margin on BA-2motifs and NCI1.

Since, AUC evaluation requires that the explanation method outputs the importance weights for the edges of a noisy sample G' , we cannot use this for comparing approaches like SubgraphX and PGM-Explainer that do not provide this information. Therefore, to provide a more comprehensive comparison, we use node accuracy as a measure to compare all the baselines. For calculating node accuracy, we consider top- k important nodes in the explanation for the original graph G as ground-truth and compare them with the top- k important nodes obtained through the explanation for the

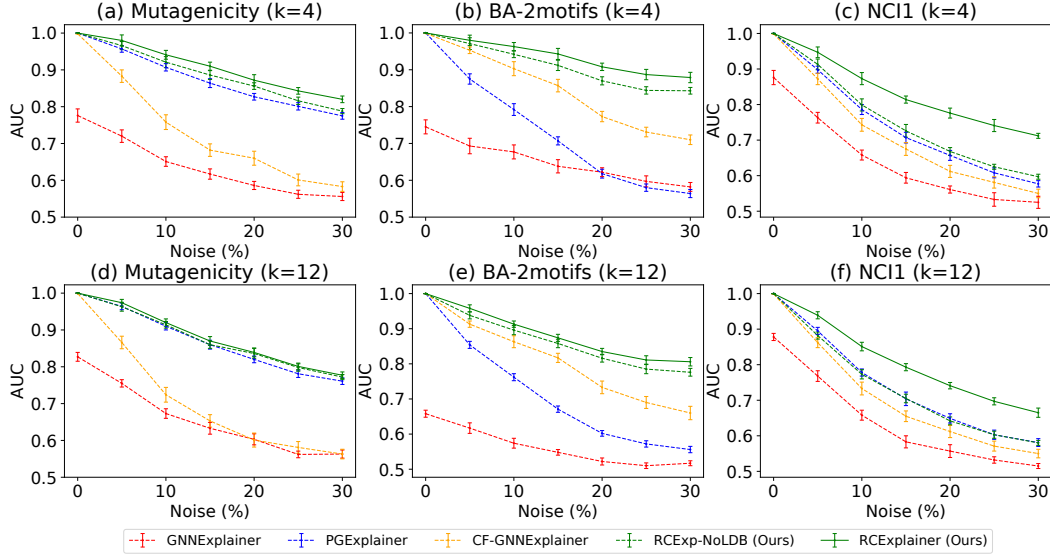


Figure 5: Noise robustness (AUC) averaged across 10 runs for the datasets at different levels of noise.

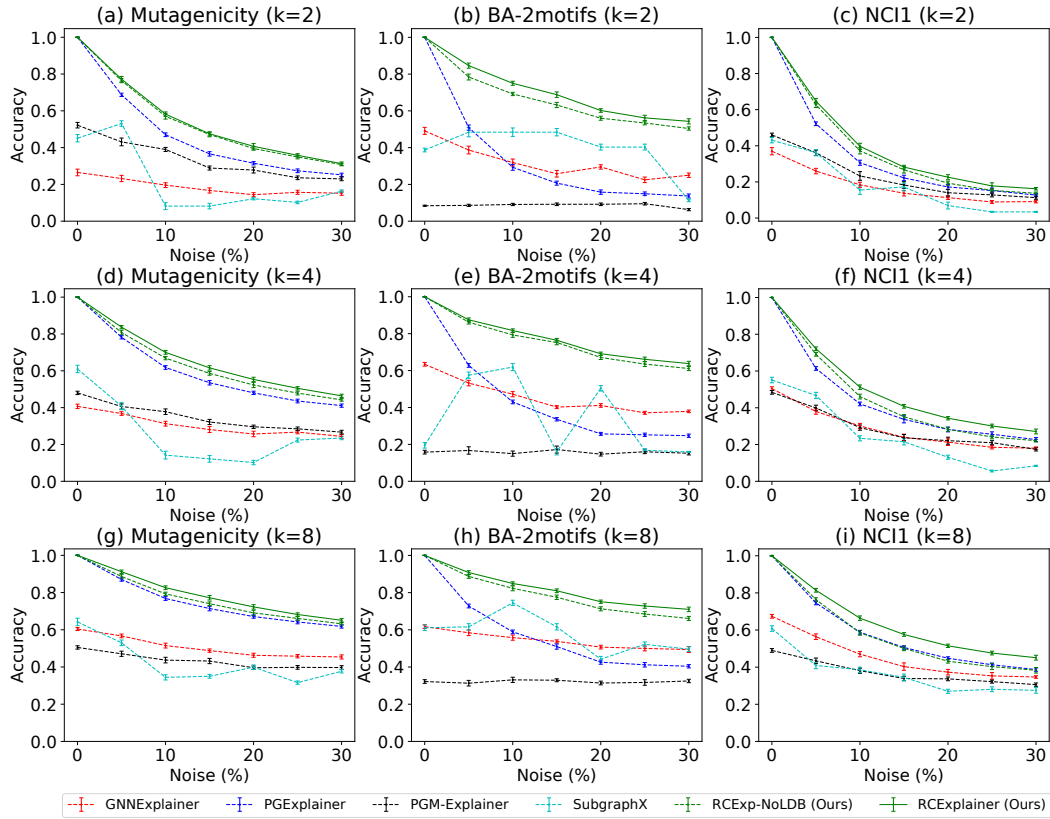


Figure 6: Noise robustness (node accuracy) averaged across 10 runs for the datasets at different levels of noise.

noisy graph G' . However, the challenge is that GNNExplainer, PGExplainer, RCExp-NoLDB and RCExp (Ours) do not rank nodes based on their importance. To address this, we use edge weights to

obtain the node weights. We approximate the node weights as :

$$\mathbf{a}_i = \max_{j \in \{1, \dots, |V|\}} (\mathbf{M}_{ij}), \quad (19)$$

where \mathbf{a}_i denotes the weight of the node v_i and \mathbf{M} is the weighted adjacency mask predicted by f_θ . We believe this is a valid approximation because for an important edge to exist in the explanation subgraph, nodes connected by this edge must also be considered important and be present in the explanation subgraph. Now, using these node weights, we can obtain the ground-truth set of nodes by picking top- k important nodes of the explanation on G . Comparing top- k important nodes of explanation on G' with the ground-truth set of nodes gives us accuracy.

We present the node accuracy plots for $k = 2, 4$ and 8 in Figure 6. We also note that comparison is not completely fair to GNNExplainer, PGExplainer and our method because of the approximation used to extend these methods for computing node level accuracy. Despite the approximation, our method significantly outperforms all the methods. GNNExplainer, PGM-Explainer and SubgraphX do not perform very well because they optimize each sample independently to obtain an explanation.

Node classification.

	BA-SHAPES		BA- COMMUNITY		TREE-CYCLES		TREE-GRID	
	AUC	Acc	AUC	Acc	AUC	Acc	AUC	Acc
GNNExplainer	0.925	0.729	0.836	0.750	0.948	0.862	0.875	0.741
PGExplainer	0.963	0.932	0.945	0.872	0.987	0.924	0.907	0.871
PGM-Explainer	<i>n.a.</i>	0.965	<i>n.a.</i>	0.926	<i>n.a.</i>	0.954	<i>n.a.</i>	0.885
CF-GNNExplainer	<i>n.a.</i>	0.960	<i>n.a.</i>	<i>n.a.</i>	<i>n.a.</i>	0.940	<i>n.a.</i>	0.960
RCEExplainer (Ours)	0.998	0.973	0.995	0.916	0.993	0.993	0.995	0.974
	± 0.001	± 0.003	± 0.002	± 0.009	± 0.003	± 0.003	± 0.002	± 0.005

Table 3: AUC and accuracy evaluation on synthetic node classification datasets.

We evaluate our method on four synthetic node classification datasets used by GNNExplainer [45], namely, BA-SHAPES, BA-COMMUNITY, TREE-CYCLES and TREE-GRID. Following [45, 25], we formalize the explanation problem as binary classification of edges and adopt AUC under the ROC curve as the evaluation metric. This evaluation is only possible for synthetic datasets where we can consider the motifs as reasonable approximations of the explanation ground truth. The edges that are part of a motif are positive and rest of the edges are labelled negative during the evaluation. We show the results in Table 3 where we demonstrate that our method is extremely accurate and achieves close to optimal score for AUC on all of the datasets. This is solid evidence of our method’s ability to capture the behavior of underlying GNN better and produce consistently accurate explanations to justify the original predictions. Please note that PGM-Explainer does not provide edge weights so it is not applicable for AUC. Also since the implementation of CF-GNNExplainer is not available, we only report those results that are available in [24].

G Hyperparameter analysis

Number of LDBs.

As mentioned in Section 4, we sample LDBs from the decision logic of GNN to form a candidate pool from which some boundaries are selected by the greedy method. In Figure 7, we show the effect of number of sampled candidate boundaries on the performance on BA-Community dataset. As we increase the number of sampled LDBs from 10 to 50, the fidelity improves and saturation is achieved once 50 LDBs are sampled. This is consistent with the expectations as more boundaries are sampled, the quality of decision region improves. When there are enough boundaries that can result in a good decision region after greedy selection, the performance saturates.

Choosing λ .

in Figure 8, we show the effect of λ hyperparameter introduced in Equation (8). We show the fidelity performance of our method on BA-2motifs dataset for different values of λ ranging from 0.01 to 0.90. The fidelity results are worst for $\lambda = 0.9$ as the second term \mathcal{L}_{opp} of the loss that enforces counterfactual behavior of explanations is weighted very less in the combined loss. Setting $\lambda = 0.1$ gives the best results for fidelity.

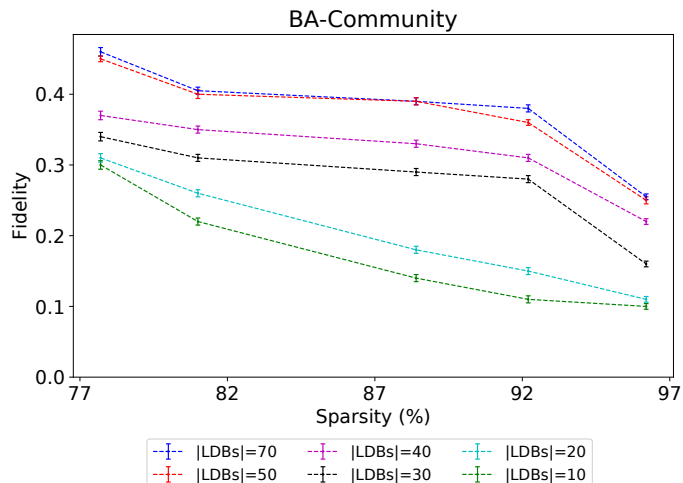


Figure 7: Fidelity vs Sparsity plots on BA-Community for different number of sampled LDBs.

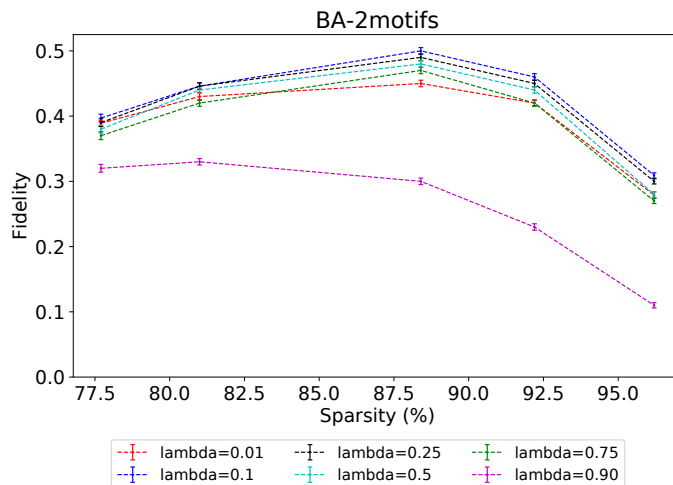


Figure 8: Fidelity vs Sparsity plots on BA-2motifs for different values of λ .

H Qualitative results

Qualitative results. We present the sample results produced by GNNExplainer, PGExplainer and RCExplainer in Table 4. Our method consistently identifies the right motifs with high precision and is also able to handle tricky cases. For instance in Figure (q), note that our method is able to identify the right motif in the presence of another “house-structure”. The other structure contains the query node but as it also contains the nodes from the other community, hence, it is not the right explanation for the prediction on the given query node. In Figure (t), our method is able to correctly identify both NO₂ groups present in the compound, and as discussed before, NO₂ groups attached to carbon rings are known to make the compounds mutagenic [6]. The edges connecting nitrogen(N) atoms to the carbon(C) atoms are given the highest weights in the explanation. This is very intuitive in counterfactual sense as masking these edges would break the NO₂ groups from the carbon ring and push the prediction of the compound towards “Non-Mutagenic”.

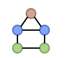

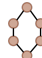
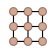
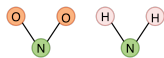

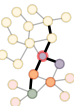

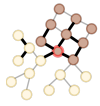
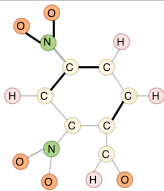

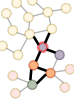

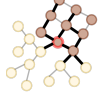
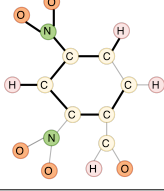


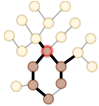

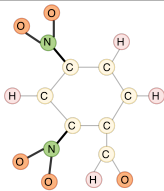
	BA-SHAPES	BA-COMMUNITY	TREE-CYCLES	TREE-GRID	Mutagenicity
Motifs	 (a)	 (b)	 (c)	 (d)	 (e)
GNNExp.	 (f)	 (g)	 (h)	 (i)	 (j)
PGExp.	 (k)	 (l)	 (m)	 (n)	 (o)
RCExp.	 (p)	 (q)	 (r)	 (s)	 (t)

Table 4: Qualitative results produced by GNNExplainer, PGExplainer and RCEExplainer. The motifs present in the corresponding dataset are shown in the first row and the corresponding explanations are shown in the later rows. First four columns correspond to node classification where the node highlighted in red is being explained and the node colors denote different labels. Last column corresponds to graph classification where the prediction is explained for a mutagenic sample and the colors denote different atoms. Explanations are highlighted in black.